Materials Advances

ROYAL SOCIETY OF CHEMISTRY

PAPER

View Article Online
View Journal | View Issue

Cite this: *Mater. Adv.*, 2024, 5, 2328

Organic fluorophore-substituted polyaza-[7]helicenes derived from 1, 10-phenanthroline: Studying the chromophoric effect on fluorescence efficiency†

B. Yadagiri,[ab] Vinay Kumar[ab] and Surya Prakash Singh *[ab]

Received 23rd November 2023,
Accepted 3rd January 2024

DOI: 10.1039/d3ma01045g

rsc.li/materials-advances

We report a series of fluorescent ''push–pull'' helicenes based on aza-[7]helicenes denoted as **AZA-FLU**, **AZA-NPC**, **AZA-TPA**, and **AZA-2OMe** for the control of the excited-state dynamics and circular dichroism properties of parent aza-[7]helicene. These symmetrical materials consist of an aza-[7]helicene central unit acting as an acceptor, which is covalently linked with different donor units, such as fluorene, *N*-phenyl carbazole, triphenylamine, and *N*,*N*-dimethoxy triphenylamine, and induces a strong ''push–pull'' character. Optoelectronic and electron distribution properties are briefly discussed in terms of electrochemical measurements and theoretical calculations. As compared to parent aza-[7]helicene (ϕ = 39% in neutral media), **AZA-NPC** shows a higher fluorescence quantum yield (ϕ = 71%) and fluorescence lifetime (τ_2 = 15.5 ns) due to the strong donating and intramolecular charge transport properties of the *N*-phenyl carbazole unit. Further, the basic nature of all aza-[7]helicenes was analyzed *via* acid titration with trifluoroacetic acid. Among them, **AZA-NPC** showed a significant change in photophysical properties, indicating a high basic nature due to the strong electron donor behavior of the *N*-phenyl carbazole unit.

Introduction

Helicenes are molecules comprising successive *ortho*-fused benzenoid rings in a helicoidal structure, and the well defining property of a helicene is its chiral helical topology.[1,2] The potential applications of chirality have been employed in multiple fields such as asymmetric synthesis, circularly polarized luminescence, surface chemistry, and optoelectronic devices.[3] Recently, hetero-helicenes that consist of one or more heteroatoms in the helicene backbone have been well explored.[4,5] Aza-helicenes are one of the most important series of hetero-helicenes because the lone pair electrons of nitrogen (N) atoms offer the possibility of coordination or protonation and improve chiroptical properties.[6] To date, a wide variety of aza-helicenes have been reported by the incorporation of nitrogen based heterocycles such as pyridine,[7] imidazolium,[8] pyrazine,[9] pyrazole,[10] and pyrrole rings.[11] However, most aza-helicenes face a significant drawback in luminescence applications due to their poor fluorescence and fluorescence quantum yields caused by rapid intersystem crossing from the singlet state to the triplet state.[12] Therefore, it is mandatory to synthesize aza-helicenes having high fluorescence quantum yield for application in optoelectronics.

Aza-helicenes with donor (D)–acceptor (A) ''push–pull'' structures are the best choice of materials to improve optical activity, emission properties, and redox activity. Push–pull aza-helicenes have been relatively rare in scientific literature; however, they have recently received significant attention owing to the unique combination of improved chirality and the essential properties of delocalized π-electron units prepared with D and/or A units.[13–15] Several research groups have made progress in their synthesis and applied them in various fields, such as dye-sensitized solar cells,[16] circularly polarized luminescence,[17] self-assembly,[18] perovskite solar cells (PSCs),[19–24] and organic light-emitting diodes (OLEDs).[25] To illustrate the most recent achievements in aza-helicenes (Fig. 1), Filip Teply reported push–pull type dicationic helical dyes (**I**) and (**II**) with prominent chiroptical properties. There are multiple advantages to these materials, including a single-step Knoevenagel condensation synthesis, ease of purification, very intense electronic circular dichroism (ECD) responses, and efficient pH-switching due to a unique combination of a cationic hemicyanine chromophore with chromophoric dyes.[26] Sun's group studied an aza-helicene

[a] *Department of Polymers and Functional Materials, CSIR-Indian Institute of Chemical Technology, Uppal Road, Tarnaka, Hyderabad 500007, Telangana, India. E-mail: spsingh@iict.res.in*
[b] *Academy of Scientific and Innovative Research (AcSIR), Ghaziabad 201002, Uttar Pradesh, India*

† Electronic supplementary information (ESI) available. See DOI: https://doi.org/10.1039/d3ma01045g

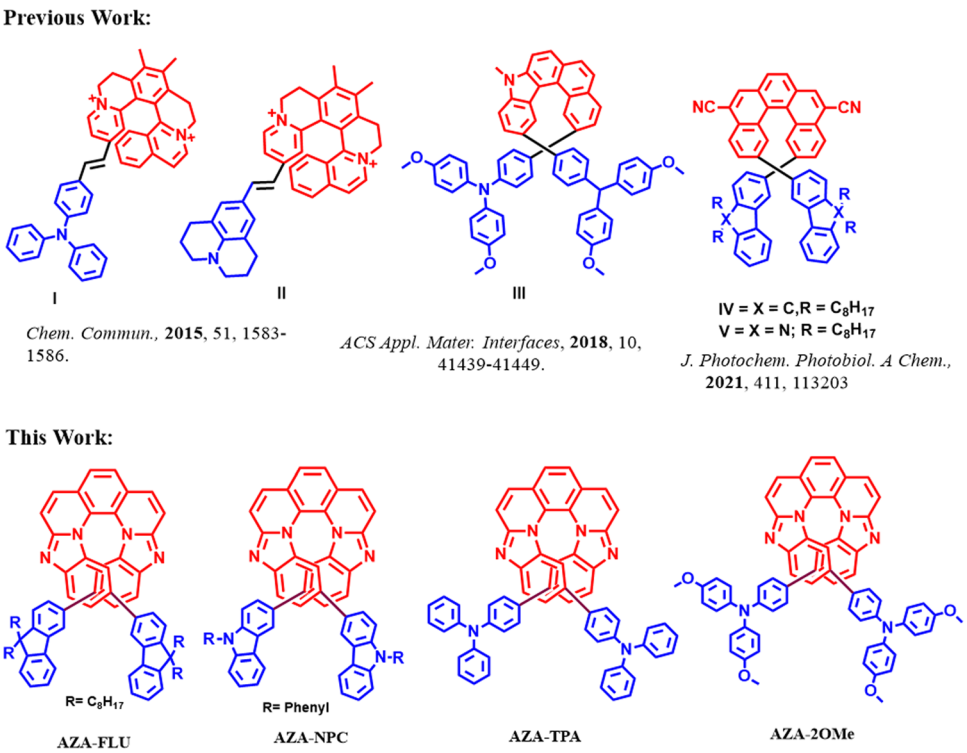

Fig. 1 Previously reported push–pull aza-helicenes and the ones from this work.[26–28]

derivative (**III**) as a hole-transporting material (HTM) for perovskite solar cells (PSCs). Owing to the appropriate energy levels of MAPbI3 perovskite, it resulted in a power conversion efficiency (PCE) of 17.34% with high ambient long-term stability up to 500 hours, as compared to spiro-OMeTAD.[27]

Our group reported a photochemical synthesis of two new fluorene and carbazole-based 2,12-disubstituted [5]helicenes (**IV**) and (**V**) for sensing (Fe^{3+}) and security applications;[28] for these materials a high fluorescence quantum yield (Φ_f) = 27% and 30%, and lifetime $\langle\tau_f\rangle$ = 9.7 ns and 4.2 ns, respectively, were observed. Several synthetic routes were developed in past decades including Diels–Alder reaction, Pd-mediated cross-coupling reactions,[29] Friedel–Crafts-type reaction,[30] metathesis reaction,[31] C–H activation,[32] radical cyclizations,[33] and [2+2+2] cyclo-addition reaction.[34]

Here, we report a facile synthesis of push–pull aza-[7]helicenes with three-step synthesis (N–H coupling, intramolecular N–H oxidative coupling, and C–C bond formation) and rare 6-5-6-6-6-5-6 skeleton from 1,10-phenanthroline. A molecular design for luminescent aza-[7]helicenes named as 10,15-bis(9,9-dioctyl-9*H*-fluoren-3-yl)benzo[4,5]imidazo[1,2-*a*]benzo[4,5]imidazo[2,1-*k*][1,10]phenanthroline (**AZA-FLU**), 10,15-bis(9-phenyl-9*H*-carbazol-3yl)benzo[4,5]imidazo[1,2-*a*]benzo[4,5]imidazo[2,1-*k*][1,10]phenanthroline (**AZA-NPC**), 4,4′-(benzo[4,5]imidazo[1,2-*a*]benzo[4,5]imidazo[2,1-*k*][1,10]phenanthroline-10,15-diyl)bis(*N*,*N*-diphenylaniline) (**AZA-TPA**) and 4,4′-(benzo[4,5]imidazo[1,2-*a*]benzo[4,5]imidazo[2,1-*k*][1,10]phenanthroline-10,15-diyl)bis(*N*,*N*-bis(4-methoxyphenyl)aniline) (**AZA-2OMe**). In the molecular design (Fig. 1), the central unit aza-[7]helicene acts as an acceptor, covalently disubstituted with various chromophoric donor units; fluorene (FLU), *N*-phenyl carbazole (NPC), triphenylamine (TPA), *N*,*N*-dimethoxy triphenylamine (2OMe) induced the great "push–pull" character. The significant effect of the chromophoric donor units on aza-[7]helicene were analysed by electrochemical studies and density functional theory (DFT) calculations. Both **AZA-TPA** and **AZA-2OMe**, showed broad absorption and emission representing high push–pull behaviour, and have suitable band gap (E_g) values, which can be utilized as HTMs in PSCs. **AZA-NPC** exhibited a high fluorescence quantum yield (ϕ = 71%) and fluorescence lifetime (τ_2 = 15.5 ns) due to strong donating ability, a higher degree of conjugation, and intramolecular charge transport properties (ICT) behaviour of the NPC unit.

Results and discussion

Synthesis and characterization

Synthetic procedures of all target molecules are briefly explained in the ESI† (Scheme S1). The desired materials were synthesized from the commercially available 1,10-phenanthroline. 2,9-Dichloro-1,10-phenanthroline (**4**) was synthesized following previous literature.[35,36] 1,10-Phenanthroline was subjected to nucleophilic substitution reaction resulting in the intermediate **2** in good yield. Compound **3** resulted from the oxidation reaction of intermediate **2** in the presence of potassium *tert*-butoxide in good yield. The 2,9-dichloro-1,10-phenanthroline (**4**) was synthesized by the activated chlorine formation reaction of compound **3** with $POCl_3$ and PCl_5 in very good yield. Then, compound **5** was synthesized by the

C–N bond formation reaction from 4-bromo aniline and 2, 9-dichloro-1,10-phenanthroline at 160 °C in solvent-free conditions with 85% yield. The prominent 10,15 dibromo aza-[7]helicene results from the hypervalent iodine reagent generated *in situ* with 4-iodoanisole and *m*-chloroperoxybenzoic acid (mCPBA) in the presence of 1,1,1,3,3,3-hexafluoro-2-propanol (HFIP) as a solvent with 21% yield.

Finally, the desired molecules **AZA-FLU**, **AZA-NPC**, **AZA-TPA**, and **AZA-2OMe** were prepared by the Suzuki cross-coupling reaction using 2 M Na_2CO_3 as a base and $Pd(PPh_3)_4$ as a catalyst obtained with moderate-good yield. Column chromatography using silica gel (60–120, 100–200, and 230–400 mesh size) was used for the purification of all the target molecules and intermediates. All the intermediates and target final compounds were fully characterized by ^{1}H-NMR, ^{13}C-NMR, and MALDI-TOF analysis. These materials are highly soluble in common organic solvents, such as dichloromethane (DCM), dimethyl sulfoxide (DMSO), dimethylformamide (DMF), and chloroform ($CHCl_3$). The spectrometry details of all compounds are provided in the ESI.†

To understand the push–pull behavior of synthesized aza-[7]helicene in terms of optoelectronic properties, the UV-visible absorption spectra were collected in the dry $CHCl_3$ solution at room temperature. The UV-vis absorption and molar extinction coefficient spectra of all aza-[7]helicenes are shown in Fig. 2a. The UV-vis absorption spectra of **AZA-FLU**, **AZA-NPC**, **AZA-TPA**, and **AZA-2OMe** have similar absorption patterns in the UV (higher energy region) to the visible region (lower energy region) (300–600 nm). **AZA-FLU** and **AZA-NPC** showed one absorption peak in the higher energy region with high intensity at 319 and 335 nm, respectively, due to weak π–π interactions within the molecule. Interestingly, **AZA-FLU** and **AZA-NPC** exhibited multiple absorption peaks in lower energy regions 391, 418, 453, and 483 nm, and 398, 425, 459, and 487 nm, respectively, which can be attributed to strong intramolecular charge transfer between the donor (fluorene and carbazole) to acceptor aza-[7]helicene. Compared to the absorption of **AZA-FLU**, the **AZA-NPC** absorption was red-shifted ~10 nm in both regions. This phenomenon can be attributed to the robust electron donation and electron-rich characteristics of the carbazole unit.

However, in the case of **AZA-TPA** and **AZA-2OMe**, the absorption spectra exhibited a single absorption peak at 347 and 353 nm, as well as in the lower energy region at 459 and 470 nm, respectively, due to strong intramolecular charge transfer. Additionally, the absorption peaks are tailing up to 550 nm due to the strong electron donation character/push–pull behavior of the triphenylamine groups, in contrast to fluorene and carbazole units. The optical band gap (E_{0-0} = $1242/\lambda_{onset}$) in the solution state is for **AZA-FLU** (2.44 eV), **AZA-NPC** (2.43 eV), **AZA-TPA** (2.37 eV), and **AZA-2OMe** (2.22 eV), which are obtained from onset-wavelength (λ_{onset}) absorption

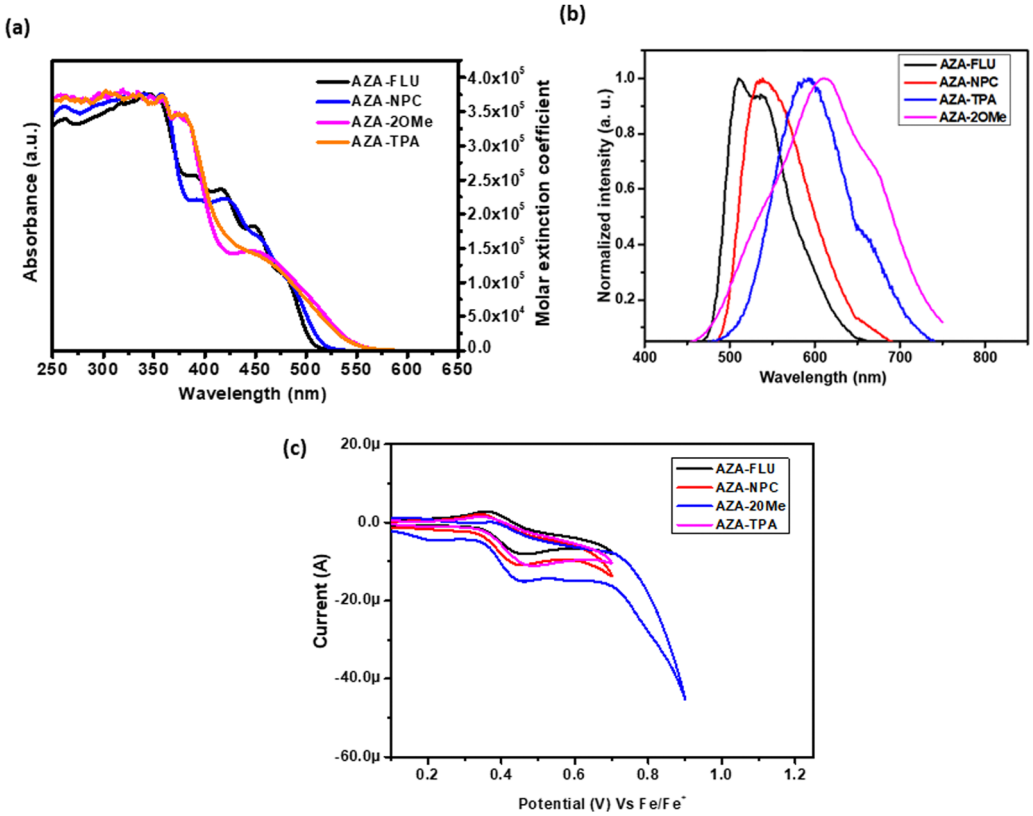

Fig. 2 (a) Normalized absorption and molar extinction coefficient spectra and (b) photoluminescence spectra of aza-[7]helicenes in dry $CHCl_3$ solution. (c) Cyclic voltammetry spectra of aza-[7]helicenes in dry DCM solution.

Table 1 Optoelectronic properties of aza-[7]helicenes

Compound	λ_{max}(abs) (nm) ($\varepsilon = 1 \times 10^{-5}$ cm^{-1} M^{-1})[a]	λ_{onset} (nm)	E_{0-0}[b] (eV)	λ_{max}[c] (nm) (emission)	E_{ox} (eV)	HOMO[d] (eV)	LUMO[e] (eV)	ϕ (%)
AZA-FLU	453(9735), 483(6288)	508	2.44	524	0.40	5.20	2.76	38
AZA-NPC	459(7086), 487(4682)	510	2.43	539	0.41	5.21	2.74	71
AZA-TPA	459(10 502)	524	2.37	590	0.43	5.23	2.86	24
AZA-2OMe	470(14 236)	558	2.22	611	0.44	5.24	3.02	53

[a] Absorption maximum in solution. [b] Band gap = $1242/\lambda_{onset}$. [c] Emission maximum. [d] HOMO = $-e[E_{ox} - 4.8(Fe^{+}/Fe)]$ (eV). [e] LUMO = $-e[E_{red} - 4.8(Fe^{+}/Fe)]$.

from absorption spectra and the detailed experimental results are tabulated in Table 1. Therefore, the obtained results suggest that the synthesized aza-[7]helicenes have suitable band gap, and absorption behavior for various optoelectronic applications such as solar cell and OLED applications.[27]

To understand the excitation and intramolecular charge transfer for **AZA-FLU**, **AZA-NPC**, **AZA-TPA**, and **AZA-2OMe**, the fluorescence emission spectra were collected in dry $CHCl_3$ solution. As shown in Fig. 2b, all aza-[7]helicene materials show single emission maximum **AZA-FLU** (524 nm), **AZA-NPC** (539 nm), **AZA-TPA** (590 nm), and **AZA-2OMe** (611 nm). The emission maximum of **AZA-TPA** and **AZA-2OMe** were red-shifted due to the strong push–pull character, which results in the strong intramolecular charge transfer between the donor (triphenylamine) to acceptor aza-[7]helicene. Noticeable changes in molecular absorption and fluorescence emission spectra were observed due to the change in the structure of the ground and excited state of aza-[7]helicenes. Furthermore, the fluorescence quantum yield (ϕ) was calculated for **AZA-FLU**, **AZA-NPC**, **AZA-TPA**, and **AZA-2OMe** in neutral media, using anthracene (ANS) (ϕ = 0.28 in EtOH) as reference dye and ϕ = 38%, 71%, 24% and 53%, were obtained, respectively. Surprisingly, **AZA-NPC** (ϕ = 71%) and **AZA-2OMe** (ϕ = 53%) showed high fluorescence quantum yield, due to the strong donating behavior of carbazole and the substituted triphenylamine group.

Furthermore, the highest occupied molecular orbitals (HOMO) and lowest unoccupied molecular orbitals (LUMO) of **AZA-FLU**, **AZA-NPC**, **AZA-TPA**, and **AZA-2OMe** were measured using cyclic voltammetry (CV) in dry DCM solution under inert atmosphere conditions (Fig. 2c). All the synthesized aza-[7]helicene showed only oxidation potentials (E_{ox}) 0.40, 0.41, 0.43, and 0.44 eV respectively. The HOMO energy levels of aza-[7]helicenes were determined to be −5.20, −5.21, −5.23 and −5.24 eV, calculated from $E_{HOMO} = -e[E_{ox} + 4.80 - E(Fc/Fc^{+})]$. The corresponding LUMO energy levels were determined to be −2.76, −2.74, −2.86 and −3.02 eV, calculated from the $E_{LUMO} = E_{HOMO}{-}E_g$ equation. Fig. 3a shows the HOMO and

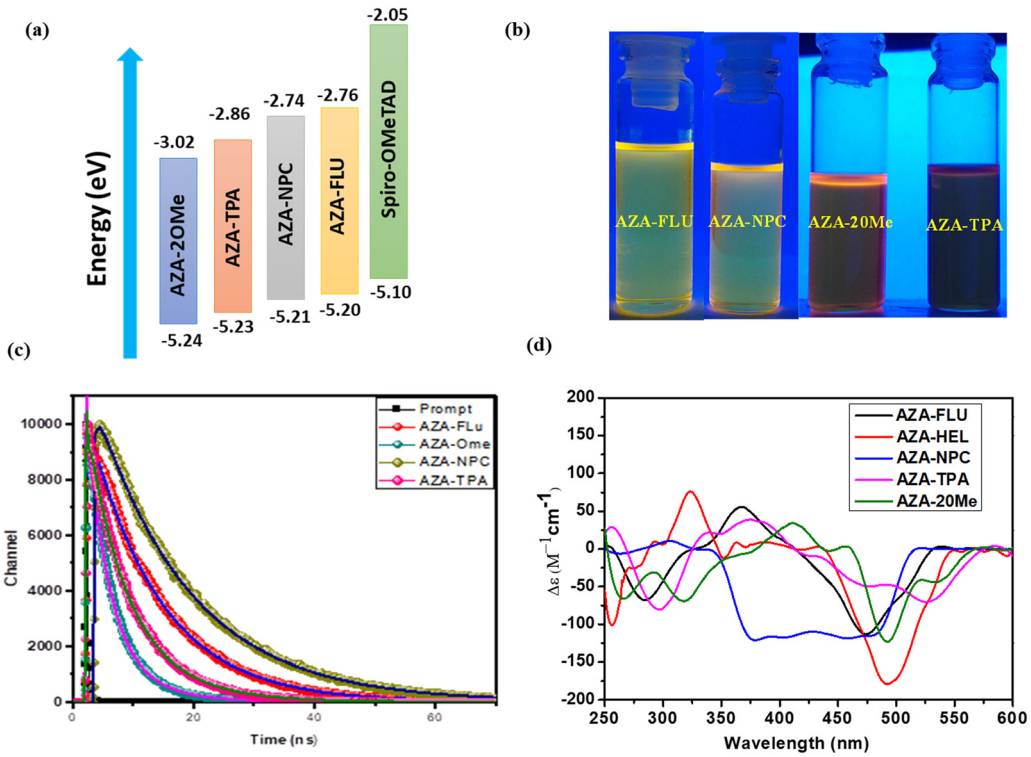

Fig. 3 (a) Energy levels comparison of aza-[7]helicenes with spiro-OMeTAD. (b) Fluorescence variation of synthesized aza-[7]helicenes substituted with different organic fluorophores. (c) Time-resolved photoluminescence spectra of helicene in dichloromethane. (d) Circular dichroism (CD) spectra of synthesized aza-[7]helicenes.

LUMO comparison of **AZA-FLU**, **AZA-NPC**, **AZA-TPA** and **AZA-2OMe** using spiro-OMeTAD (2,2′,7,7′-tetrakis(*N*,*N*′-di-*p*-methoxyphenylamine)-9,9′-spirobifluorene) as a well-known hole transporting material (HTM) for PSCs. This indicates that all the aza-[7]helicenes are suitable for the hole transporting process in PSCs applications.[36,37] Thus, the introduction of fluorene, carbazole and triphenylamine units on aza-[7]helicene can improve several optoelectronic properties, such as quantum yield, maximum wavelength (λ_{max}), molar extinction coefficient (ε), band gap (E_g) and fluorescence emission (λ_{em}) of molecules, due to strong push–pull effect between the donor and aza-[7]helicene moiety.

To understand the stability of the ground state and excited state structures of aza-[7]helicenes in different polarities of solvents. The solvatochromism experiment was performed in different polarity solvents such as $CHCl_3$, DCM, DMF, ethyl acetate (EA), and toluene (TOL). The UV-visible absorption and emission spectra are represented in ESI† (Fig. S1 and S2) and corresponding values are tabulated in Table S1 (ESI†). The absorption spectra of all aza-[7]helicenes are less sensitive towards the solvent polarity, which indicates that the interaction of dyes with solvents in the ground state is less significant. However, the emission spectra are red-shifted by ~20 nm due to the most polar excited states and strong intramolecular charge transfer process. Hence, observation indicates that the excited states of aza-[7]helicenes are more polar than their ground states. Generally aza-[7]helicenes are basic in nature because of multiple nitrogen atoms within the fused helicene.[38] As such, when substituted with a strong electron donor triphenylamine it can enhance the basicity of the molecule and change the fluorescence property (Fig. 3b). The change in fluorescence behaviour in different solvents is shown in Fig. S3 (ESI†). In the presence of most polar solvents such as DMF, the emission intensity is slowly reduced and redshifted because of the neutralization effect with the basic nature of aza-[7]helicenes and the acidic character of DMF.

To understand the fast or slower charge carrier dynamics of push–pull helicenes in the nanosecond to the microsecond, the time-correlated single photon counting (TCSPC) technique was performed and the results are shown in Fig. 3c. All aza-[7]helicenes show bi-exponential decay kinetics when studied at their emission maximum in dry $CHCl_3$ solution using wavelength 375 nm nano-LED as the excitation source. The details of photoluminescence decay fitting parameters are shown in Table S2 in the ESI.† The **AZA-NPC** (τ_1 = 7.76 ns, τ_2 = 15.5 ns) and **AZA-FLU** (τ_1 = 5.69 ns, τ_2 = 11.44 ns) show high lifetime when compared with other aza-[7]helicenes due to strong fluorescence property of *N*-phenyl carbazole and fluorene donor units, respectively.

To understand the basic nature of **AZA-FLU**, **AZA-NPC**, **AZA-TPA**, and **AZA-2OMe**, we performed the acid titration experiment with trifluoroacetic acid (TFA) and observed the effect of TFA on their photophysical properties (Fig. S4 and S5, ESI†). Prior to the addition of *ca.* 0.45 M of TFA to the solution of aza-[7]helicene, a significant change was observed in absorption and emission spectra. The absorption peak intensities of **AZA-FLU**, **AZA-NPC**, **AZA-TPA**, and **AZA-2OMe** at 348, 335, 335, and 355 nm gradually decreased and redshifted to 355, 353, 371, and 377 nm while increasing the concentration of the TFA solution. New absorption peaks located at 376 and 408 nm were observed upon the titration of **AZA-NPC** and **AZA-TPA** with TFA concentrations from 0.05 M to 0.45 M compared to **AZA-FLU** and **AZA-2OMe.** In the case of emission spectra, the emission intensity was drastically reduced and redshifted. As compared to **AZA-FLU**, materials **AZA-NPC**, **AZA-TPA**, and **AZA-2OMe** showed negligible emission intensity with successive amounts of 0.05 M, due to the more basic nature arising from strong donors, such as carbazole and triphenylamine units. This result suggested that when aza-[7]helicenes are substituted with strong electron donor chromophores, the basic nature phenomenon increases and is sensitive to acidic substances.

The chiroptical property is a primary observation of helicene molecules, as such, we obtained circular dichroism (CD) spectra for the synthesized aza-[7]helicenes, in dry $CHCl_3$ solution (Fig. 3d), with a solution concentration of 3×10^{-5} M^{-1} cm^{-1}. The parent aza-[7]helicene (**AZA-HEL**) showed one positive cotton band at 323 nm ($\Delta\varepsilon$ = 79 M^{-1} cm^{-1}) and a very strong cotton band at 492 nm ($\Delta\varepsilon$ = 182 M^{-1} cm^{-1}). However, in the case of substituted aza-[7]helicenes, such as **AZA-FLU**, **AZA-NPC**, **AZA-TPA**, and **AZA-2OMe**, cotton bands were red-shifted by ~40–90 nm, those are 367 nm ($\Delta\varepsilon$ = 57 M^{-1} cm^{-1}), 343 nm ($\Delta\varepsilon$ = 2 M^{-1} cm^{-1}), 378 nm ($\Delta\varepsilon$ = 39 M^{-1} cm^{-1}) and 412 nm ($\Delta\varepsilon$ = 37 M^{-1} cm^{-1}) in the higher energy region likely arising from the central helicene moiety and strong cotton bands at 473 nm ($\Delta\varepsilon$ = 112 M^{-1} cm^{-1}), 481 nm ($\Delta\varepsilon$ = 115 M^{-1} cm^{-1}), 525 nm ($\Delta\varepsilon$ = 71 M^{-1} cm^{-1}) and 493 nm ($\Delta\varepsilon$ = 125 M^{-1} cm^{-1}), respectively, in the lower energy region as the strong absorptivity of fluorene, carbazole, and triphenylamine chromophores results in inherent chirality of aza-[7]helicenes.

The density functional theory (DFT) calculations were computed to understand the structural, electronic, and charge transport properties of **AZA-FLU**, **AZA-NPC**, **AZA-TPA**, and **AZA-2OMe** using B3LYP exchange correlations functional with 6-311g(d,p) as the basis set in Gaussian 09 programs.[39] To better understand the solvation effect of all aza-[7]helicenes, the self-consistent reaction field (SCRF) calculation was performed using a conductor-like polarizable continuum model (CPCM). The optimized geometry of **AZA-FLU**, **AZA-NPC**, **AZA-TPA**, and **AZA-2OMe** helicenes are shown in Fig. 4. The optimized geometry of all aza-[7]helicenes shows a highly twisted non-planar molecular geometry, in which fluorene, carbazole, triphenylamine, and methoxy-substituted triphenylamine units are twisted out of the plane, promoting the solubility of aza-[7]helicenes in common organic solvents, thereby making a very smooth thin film for application in variety of optoelectronic properties.

The HOMOs of **AZA-FLU** and **AZA-NPC** are distributed throughout the central aza-[7]helicene core, fluorene, and carbazole units. However, in the case of **AZA-TPA** and **AZA-2OMe** the HOMOs are strongly distributed into the triphenylamine and methoxy-substituted triphenylamine end cap units, indicating the rapid creation of neutral excitons and the transition of hole transfer due to strong push–pull property of aza-[7]helicenes

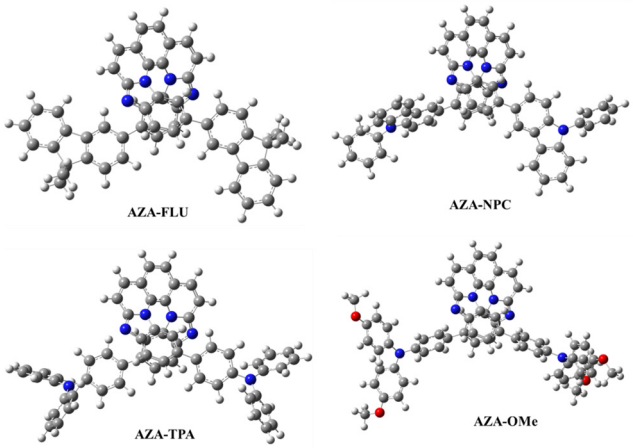

Fig. 4 The optimized structures of **AZA-FLU**, **AZA-NPC**, **AZA-TPA**, and **AZA-2OMe** helicenes.

(Fig. 5a). A trend in lowering the E_g value was obtained from the substitution of fluorene (3.04 eV), carbazole (2.80 eV), triphenylamine (2.61 eV) to methoxy substituted triphenylamine (2.35 eV) units at aza-[7]helicene core that indicated the strong push–pull behavior in **AZA-2OMe**, which can induce the ICT property. The deeper HOMO energy levels of **AZA-FLU**, **AZA-NPC**, **AZA-TPA**, and **AZA-2OMe** also suggest that they can be utilized as a hole transporting material (HTM) for PSCs (Fig. S6, ESI†). The electrostatic surface potential (ESP) (Fig. 5b) reveals the electronegative character of the nitrogen in **AZA-FLU**, **AZA-NPC**, **AZA-TPA**, and **AZA-2OMe** present on the aza-[7]helicene core, while the most electropositive portion is much more spread out over the molecule. Among them, **AZA-TPA** and **AZA-2OMe** exhibited a stronger electronegative character at the nitrogen of the aza-[7]helicene core. Therefore, **AZA-TPA** and **AZA-2OMe** showed much higher sensitivity toward acid when we performed the acid titration experiment with TFA, as discussed above.

To compare the experimental absorption results with the theoretical data, the time-dependent density functional theory (TD-DFT) method was used by considering similar exchange–correlation functional and basis sets in Gaussian 09 programs. The geometric parameters of all aza-[7]helicene in the singlet state reproduce the experimental values. To cover the ultraviolet region (300 nm) to the visible region (600 nm) of aza-[7]helicenes 30 excitations were performed. We mainly concentrated on the visible region to examine the charge transfer. The theoretical absorption spectra of all aza-[7]helicenes are in alignment with the experimental results.

Conclusions

We synthesized a series of symmetric aza-[7]helicenes, denoted as **AZA-FLU**, **AZA-NPC**, **AZA-TPA**, and **AZA-2OMe** with a 6-5-6-6-6-5-6 helicene skeleton, from 2,9-dichloro-1,10-phenanthroline through double amination followed by intramolecular double-NH/CH and Suzuki–Miyaura coupling processes. The optoelectronic and electron distribution properties were briefly discussed in terms of electrochemical measurements and theoretical studies. These results suggested that all aza-[7]helicenes exhibited suitable optical and electrochemical properties for a variety of optoelectronic applications. The fluorescence quantum yield (ϕ) and time-correlated single photon counting in neutral media were calculated for all aza-[7]helicenes. Mostly, **AZA-NPC** showed very high fluorescence quantum yield (ϕ = 71%) and lifetime (τ_2 = 15.5 ns) because of the strong fluorophore behavior of the *N*-phenyl carbazole unit. Furthermore, the basic nature of aza-[7]helicenes analyzed by acid titration

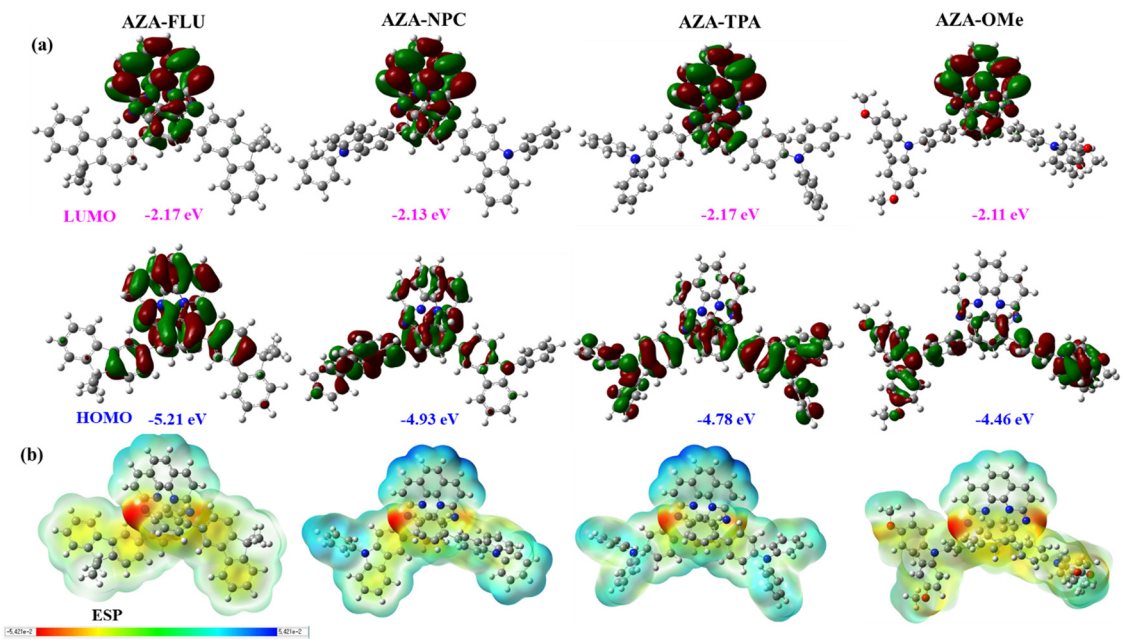

Fig. 5 (a) Molecular energy levels (HOMO and LUMO) and (b) electrostatic potential diagram (ESP) of **AZA-FLU**, **AZA-NPC**, **AZA-TPA**, and **AZA-2OMe** helicenes.

with trifluoroacetic acid, among the synthesized aza-[7]helicenes **AZA-NPC** showed good sensitivity and significant change in the photophysical properties, indicating the high basic nature due to the strong electron donor capability of the *N*-phenyl carbazole unit. Due to the interesting properties of these novel aza-[7]helicenes, they can be used as promising functional materials in future optoelectronic devices such as organic light-emitting diodes, solar cells, and mechano-chromic applications.

Conflicts of interest

There are no conflicts to declare.

Acknowledgements

B. Y. G. and S. P. S. acknowledge financial support from CSIR (Ref. no. 34/1/TD-CLP/NCP-FBR 2020-RPPBDD-TMD-Se-MI). CSIR-IICT Communication Number: IICT/Pubs./2020/284.

References

1 M. Gingras, *Chem. Soc. Rev.*, 2013, **42**, 968–1006.
2 M. Gingras, G. Félix and R. Peresutti, *Chem. Soc. Rev.*, 2013, **42**, 1007–1050.
3 M. Li, C. Zhang, L. Fang, L. Shi, Z. Tang, H.-Y. Lu and C.-F. Chen, *ACS Appl. Mater. Interfaces*, 2018, **10**, 8225–8230.
4 Y. Shen and C.-F. Chen, *Chem. Rev.*, 2012, **112**, 1463–1535.
5 K. Dhbaibi, L. Favereau and J. Crassous, *Chem. Rev.*, 2019, **119**, 8846–8953.
6 T. Taniguchi, Y. Nishii, T. Mori, K. Nakayama and M. Miura, *Chem. – Eur. J.*, 2021, **27**, 7356–7361.
7 J. Míšek, F. Teplý, I. G. Stará, M. Tichý, D. Šaman, I. Císařová, P. Vojtíšek and I. Starý, *Angew. Chem., Int. Ed.*, 2008, **47**, 3188–3191.
8 M. Čížková, D. Šaman, D. Koval, V. Kašička, B. Klepetářová, I. Císařová and F. Teplý, *Eur. J. Org. Chem.*, 2014, 5681–5685.
9 A. Abhervé, K. Martin, A. Hauser and N. Avarvari, *Eur. J. Inorg. Chem.*, 2019, 4807–4814.
10 Y. Yoshida, N. Aso, T. Karatsu, T. Mino and M. Sakamoto, *Org. Lett.*, 2023, **25**, 3412–3416.
11 G. M. Upadhyay, H. R. Talele, S. Sahoo and A. V. Bedekar, *Tetrahedron Lett.*, 2014, **55**, 5394–5399.
12 H. Oyama, M. Akiyama, K. Nakano, M. Naito, K. Nobusawa and K. Nozaki, *Org. Lett.*, 2016, **18**, 3654–3657.
13 K. Jana, D. Sarkar, P. Jaiswal and J. N. Moorthy, *J. Org. Chem.*, 2023, **88**, 6611–6622.
14 C. Qu, Y. Zhu, L. Liang, K. Ye, Y. Zhang, H. Zhang, Z. Zhang, L. Duan and Y. Wang, *Adv. Opt. Mater.*, 2023, **11**, 2203030.
15 T. Beránek, M. Kos, L. Váňa, I. Císařová, J. Sýkora, J. Storch, V. Církva and M. Jakubec, *Dyes Pigm.*, 2023, **210**, 111039.
16 D. Dova, S. Cauteruccio, N. Manfredi, S. Prager, A. Dreuw, S. Arnaboldi, P. R. Mussini, E. Licandro and A. Abbotto, *Dyes Pigm.*, 2019, **161**, 382–388.
17 K. Dhbaibi, L. Abella, S. Meunier-Della-Gatta, T. Roisnel, N. Vanthuyne, B. Jamoussi, G. Pieters, B. Racine, E. Quesnel, J. Autschbach, J. Crassous and L. Favereau, *Chem. Sci.*, 2021, **12**, 5522–5533.
18 M. Šámal, J. Rybáček, J. Holec, J. Hanus, J. Vacek, M. Buděšínský, L. Bednárová, P. Fiedler, M. Š. Slušná, I. G. Stará and I. Starý, *Chem. Commun.*, 2022, **58**, 12732–12735.
19 Z. Tang, T. Li, Y. Cao, Y. Zhang, L. He, A. Zheng and M. Lei, *ChemSusChem*, 2021, **14**, 4923–4928.
20 Y.-S. Lin, S. Y. Abate, K.-W. Lai, C.-W. Chu, Y.-D. Lin, Y.-T. Tao and S.-S. Sun, *ACS Appl. Mater. Interfaces*, 2018, **10**, 41439–41449.
21 J. Vailassery and S.-S. Sun, *Molecules*, 2023, **28**, 510.
22 Z.-Z. Sun and R. Long, *J. Phys. Chem. C*, 2023, **127**, 12913–12922.
23 M. Ren, J. Wang, X. Xie, J. Zhang and P. Wang, *ACS Energy Lett.*, 2019, **4**(11), 2683–2688.
24 X. Liu, B. Ding, M. Han, Z. Yang, J. Chen, P. Shi, X. Xue, R. Ghadari, X. Zhang, R. Wang, K. Brooks, L. Tao, S. Kinge, S. Dai, J. Sheng, P. J. Dyson, M. K. Nazeeruddin and Y. Ding, *Angew. Chem., Int. Ed.*, 2023, **62**, e202304350.
25 S. Jhulki, A. K. Mishra, T. J. Chow and J. N. Moorthy, *Chem. – Eur. J.*, 2016, **22**, 9375–9386.
26 P. E. Reyes-Gutiérrez, M. Jirásek, L. Severa, P. Novotná, D. Koval, P. Sázelová, J. Vávra, A. Meyer, I. Císařová, D. Šaman, R. Pohl, P. Štěpánek, P. Slavíček, B. J. Coe, M. Hájek, V. Kašička, M. Urbanová and F. Teplý, *Chem. Commun.*, 2015, **51**, 1583–1586.
27 Y. S. Lin, S. Y. Abate, K. W. Lai, C. W. Chu, Y. D. Lin, Y. T. Tao and S. S. Sun, *ACS Appl. Mater. Interfaces*, 2018, **10**, 41439–41449.
28 B. Yadagiri, P. J. S. Rana and S. P. Singh, *J. Photochem. Photobiol. A Chem.*, 2021, **411**, 113203.
29 M. Shimizu, I. Nagao, Y. Tomioka and T. Hiyama, *Angew. Chem., Int. Ed.*, 2008, **47**, 8096–8099.
30 H. Okubo and M. Yamaguchi, *J. Org. Chem.*, 2001, **66**, 824–830.
31 S. K. Collins, A. Grandbois, M. P. Vachon and J. Côté, *Angew. Chem., Int. Ed.*, 2006, **45**, 2923–2926.
32 C. Shen, M. Srebro-Hooper, M. Jean, N. Vanthuyne, L. Toupet, J. A. G. Williams, A. R. Torres, A. J. Riives, G. Muller, J. Autschbach and J. Crassous, *Chem. – Eur. J.*, 2017, **23**, 407–418.
33 D. C. Harrowven, M. I. T. Nunn and D. R. Fenwick, *Tetrahedron Lett.*, 2002, **43**, 7345–7347.
34 K. Tanaka, A. Kamisawa, T. Suda, K. Noguchi and M. Hirano, *J. Am. Chem. Soc.*, 2007, **129**, 12078–12079.
35 H. C. Guo, R. H. Zheng and H. J. Jiang, *Org. Prep. Proced. Int.*, 2012, **44**, 392–396.
36 P. Mäkinen, F. Fasulo, M. Liu, G. K. Grandhi, D. Conelli, B. Al-Anesi, H. Ali-Löytty, K. Lahtonen, S. Toikkonen, G. P. Suranna, A. B. Muñoz-García, M. Pavone, R. Grisorio and P. Vivo, *Chem. Mater.*, 2023, **35**, 2975–2987.
37 L. Wang, J. Zhang, P. Liu, B. Xu, B. Zhang, H. Chen, A. K. Inge, Y. Li, H. Wang, Y.-B. Cheng, L. Kloo and L. Sun, *Chem. Commun.*, 2018, **54**, 9571–9574.
38 T. Otani, A. Tsuyuki, T. Iwachi, S. Someya, K. Tateno, H. Kawai, T. Saito, K. S. Kanyiva and T. Shibata, *Angew. Chem., Int. Ed.*, 2017, **56**, 3906–3910.
39 B. Yadagiri, T. H. Chowdhury, Y. He, R. Kaneko, A. Islam and S. P. Singh, *Mater. Chem. Front.*, 2021, **5**, 7276–7285.